International Journal of Nanoelectronics and Materials
Volume 16 (Special Issue) December 2023 [33-42]

DFT Study of Borophene/Graphene (B/G) Heterostructure Properties as Sodium-Ion Battery Anode

Faozan Ahmad[1,*], Teja Alkori[1] and Husin Alatas[1,2]

[1] Theoretical Physics Division, Department of Physics, Jl. Meranti, Kampus IPB Darmaga, IPB University, Bogor 16680, Indonesia
[2] Center for Transdisciplinary & Sustainability Sciences (CTSS), IPB University, Kampus IPB Baranangsiang, Jl. Raya Pajajaran 27, Bogor 16128

ABSTRACT

As an alternative to lithium-ion batteries, sodium-ion batteries are gaining more attention as a solution to issues including the high cost and restricted supply of lithium. Nonetheless, issues including low voltage, limited capacity, and low electrode material capacity need to be fixed for sodium-ion battery applications. The proposed borophene/graphene heterostructure anode material for sodium-ion batteries was studied using density functional theory (DFT) to ascertain its properties. The findings demonstrate that there is sufficient interlayer spacing in the borophene/graphene heterostructure to allow for Na-intercalation. The interspace heterostructure has the highest Na adsorption energy of -2.02 eV. As a result, its maximum energy specific capacity is around 969.65 mAh/g. The borophene/graphene heterostructure anode exhibits strong diffusivity of Na ions, as evidenced by the activation energy of Na ion mobility in the heterostructure being less than 0.2 eV.

Keywords: Sodium-ion battery**,** heterostructure anode, borophene/graphene

1. INTRODUCTION

Developments in electronic technology and electric vehicles demand the availability of rechargeable batteries with large capacities and compact sizes. Currently, battery technology is dominated by lithium-ion batteries. 70% of lithium sources are in South America, specifically in Chile, Argentina, and Bolivia. Current lithium reserves will only last approximately 50 years after being exploited, so an alternative material is needed that can replace lithium as a future energy storage unit that has good performance, is cheap, and has abundant availability [1]. Sodium is the right candidate for creating cheap and safe batteries. Sodium is abundant in nature and has electronic properties similar to lithium. The abundance of sodium on earth is as much as 23600 ppm in the earth's crust, while lithium is only 20 ppm in the earth's crust [2, 3].

Two things of concern in the development of sodium-ion batteries are how to achieve high energy and power density. Energy density states how much energy can be stored in the battery while power density refers to how fast the battery can distribute energy. These two characteristics are often intertwined, and achieving high scores for both can be challenging because it sometimes involves trade-offs. An increase in energy density can lead to a reduction in power density, and vice versa. The main components of the battery that determine the dominant performance of the battery are the electrodes including the cathode and anode. The development of cathode and anode materials for sodium-ion batteries generally follows the development framework for lithium batteries. However, because the radius of the sodium atom is larger (1.02 Å) compared to that of the lithium atom (0.76 Å), many lithium battery electrodes are not suitable for sodium batteries [4]. So far several new electrode materials for sodium-ion

* Corresponding authors: faozan@apps.ipb.ac.id

batteries have been proposed. Cathode materials are classified according to their structure, namely sodium transition metal oxides (TMOs), polyanionic compounds, Prussian blue analogs (PBA), and organic cathodes [5,6]. The anode material consists of several material categories including carbon-based anodes (graphite carbon), hard carbon, alloy anodes, metal oxides, metal sulfides, and organic materials [7].

The carbon-based anode material (graphite) which is a commercial anode for lithium-ion batteries, does not work for sodium-ions batteries as it produces very low capacities. Modification of 2D carbon-based anodes can be carried out by forming heterostructures with large enough interlayer spacing. The incorporation of Van der Waals heterostructures consisting of different 2D materials gives rise to emergent properties that can be explored to address energy conversion and storage [8,9]. Graphene and borophene are two 2D materials that have superior electrical conductivity. 2D material has advantages in electrochemical properties because it has a large surface area and a high diffusion rate [10]. Graphene is a 2D structure of carbon which is a semiconductor material with zero bandgap and is mechanically a strong material. Meanwhile, Borophene is a 2D structure of boron which is the lightest two-dimensional metal with high anisotropy which can produce unique plasmonic and electron correlation phenomena [10]. There have been many studies of borophene-based heterostructures including borophene/MoS_2, borophene/$MoSe_2$, borophene/WS_2, borophene/silicene, borophene/blue-phosphorene, borophene/black-phosphorene, and borophene/germanene, [12-15] . Van der Waals heterostructures on the borophene/graphene (B/G) structure allow for a wide enough interlayer space for the mobility of Na ions.

In this study, the properties of B/G heterostructures as an anode of sodium-ion battery have studied computationally using the density functional theory (DFT) method. There are several things of concern, including the geometric structure of the B/G heterostructure, the interaction and adsorption of Na ions on the B/G heterostructure, the open circuit voltage, the theoretical battery capacity, and the mobility of Na ions on the B/G heterostructure.

2. COMPUTATIONAL METHODS

The Quantum Espresso program is used to do non-spin-polarized Kohn-Sham DFT computations. Based on functional PBE (Perdew-Burke-Ernzerhoff), the exchange and correlation functionals are described via the generalized gradient approximation, or GGA. Van der Vanderbilt ultrasoft pseudopotential is used to model core ions. The Brillouin zone is integrated on an 8 x 8 x 1 k-point grid sampled using the Monkhorst-Pack technique. A 500 eV cut-off energy was applied to restrict the plane-wave basis set.

2.1 Computational Model

The B/G heterostructure was obtained by stacking the 2D monolayer structures of Borophene and Graphene with supercell sizes of 3 x 3 and 2 x 2, respectively. With this supercell size, almost the same hexagonal unit cell sizes were obtained with the lattice mismatch 4.2 % as shown in Table 1.

Table 1 Lattice Parameter (Å)

Structure	***a=b***
Borophene (B)	5.13078
Graphene (G)	4.92081
Borophene/Graphene (B/G)	4.92081

2.2 Adsorption Energy

The adsorption energy of Na atoms on the B/G heterostructure is calculated using equation 1.

$$E_{ads} = \frac{E_{B/G+Na} - (E_{B/G} + E_{Na})}{n} \quad (1)$$

where $E_{B/G+Na}$, $E_{B/G}$, E_{Na}, n denote the total energies of B/G heterostructure and adsorbed atom system, the energy of clean heterostructure , energy of an isolated adsorbed atom in a vacuum, and number of Na atom, respectively. Based on this definition, negative value of E_{ads} indicates a stable adsorption.

2.3 Interaction and Electronic Properties

Heterostructure formation and the interaction of Na atoms with the heterostructure surface were analyzed based on the electronic properties of the system by calculating the density of states (DOS), projected DOS (PDOS), and charge transfer. The calculation of the charge transfer interaction between the surface of the heterostructure and the adsorbate will be based on the analysis of the Löwdin Charge Population. This charge transfer is calculated using Equation 2.

$$\Delta Q_{ads} = Q_{after\_ads} - Q_{before\_ads} \quad (2)$$

2.4 Open Circuit Voltage

The open circuit voltage (OCV) can be calculated from the adsorption energy using equation 3.

$$OCV = \frac{E_{ads}}{n\,e} \quad (3)$$

where n is number of adsorbed Na atom, and e is electron charge.

2.5 Diffusion Path

The energy diagram on the mobility of Na ions along the diffusion path is obtained by calculating the transition position (TP) between the initial position (IP) and the final position (FP). Transition state calculations were performed using the Climbing Image Nudged Elastic Band (CI-NEB) method. Activation energy is defined as a potential barrier ($E_{barrier}$) that must be passed to make the transition from the initial position to the final position calculated using Equation 4.

$$E_{barrier} = E_{TP} - E_{IP} \quad (4)$$

where $E_{barrier}$ is barrier potential, E_{TP} is the transition state energy, and E_{IP} is the initial state energy.

3. RESULTS AND DISCUSSION

The calculation begins with the optimization of the 2D structure of Borophene and Graphene separately with the supercell size as shown in Table 1. Then the two optimized structures are stacked in one cell to form a heterostructure as shown in Figure 1. The two layers are bonded quite tightly with a binding energy between layers of -2.2 eV. The B-B bond length in the Borophene layer ranges from 1.64 Å to 1 .89 Å. while the C-C bond length in the Graphene layer is 1.42 Å. The farthest distance of the B/G interlayer space is 4.9 Å and the closest is 3.8 Å (see

Figure 1a). This distance is sufficient to be intercalated by sodium atoms (with atomic diameter of 1.86 Å).

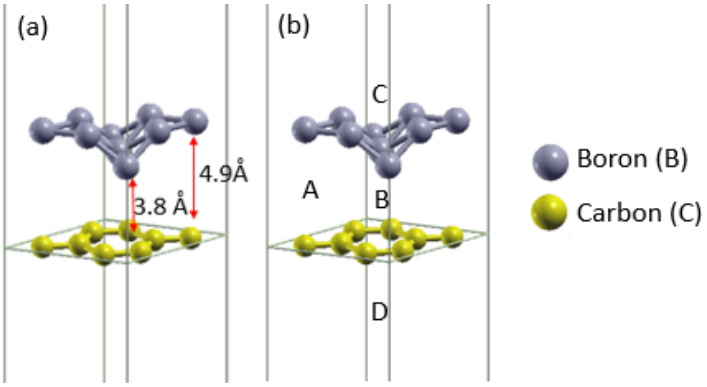

Figure 1. Optimized B/G Heterostructure: (a) interlayer distance and (b) Na adsorption sites.

3.1 Electronic Structure of B/G Hetero structure

The electronic structures of borophene and graphene, as well as B/G heterostructures, are shown in Figure 2. The density of state (DOS) of graphene, which is a semiconductor material with a bandgap of zero, is shown in Figure 2a. It appears that the valence and conduction bands coincide at the Fermi level (E = 0), forming Dirac points. The metallic property of borophene is confirmed by the DOS curve in Figure 2b. The combination of these two electronic structures produces a heterostructure with metallic properties, as shown in Figure 2c. The long-range Van der Walls electrostatic bonds between the borophene and graphene layers can be analyzed through the projected DOS (PDOS) of the constituent atoms before and after the formation of the B/G heterostructure, which is presented in Figure 2d. As shown in the figure, the C-2p orbital has shifted to the right, while the PDOS B-2p orbital has slightly shifted to the left in the heterostructure phase. This shows a change in the charge distribution, with the borophene layer having a slightly negative charge and the graphene layer having a slightly positive charge.

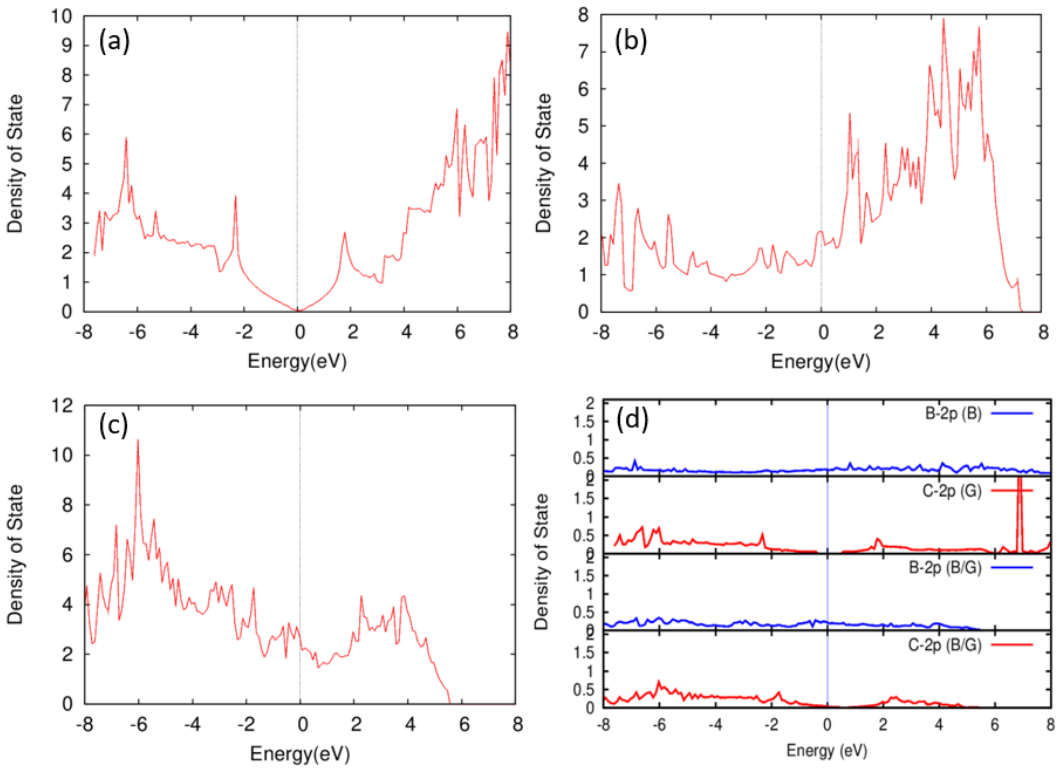

Figure 2. Electronic structure of heterostructure B/G. (a). Density of state (DOS) of graphene, (b) DOS of borophene, (c). DOS of heterostructure B/G, (d) Projected DOS of selected atomic orbitals before and after the formation of the heterostructure.

3.2 Na adsorption on B/G heterostructure

The adsorption of the Na atom on the heterostructure was studied at 4 sites, namely A, B, C, and D as depicted in Figure 1b. The adsorption energy, distance of Na from the surface atoms, and charge transfer are shown in Table 2. The strongest adsorption of Na atoms with an adsorption energy of -2.02 eV occurred at site C, namely above the borophene surface, then followed by adsorption at site A (the wide gap in the interlayer space) at -1.74 eV, adsorption at site D (below the graphene surface) at -1.21, and the weakest is the adsorption of Na at site B, namely in the narrow interlayer space of -0.29 eV. Based on the Na charge change data, it appears that the adsorbed Na tends to be fully ionized at adsorption sites A, B, and C, except for site D.

Table 2 Adsorption energy and charge transfer of Na atom on heterostructure

Adsorption site	Adsorption Energy (eV)	Na-Br (Na-Gr) (Å)	ΔQ (e)
A	-1. 74	2.58 (2.36)	-0.77
B	-0.29	2.47 (2.29)	-0.77
C	-2.02	2.58	-0.61
D	-1.21	(3.6)	-0.13

The mechanism of Na adsorption in B/G heterostructures can be explained by changes in the electronic structure before and after adsorption which are shown in Figure 3. Figure 3 displays changes or shifts in the projected DOS curves for the Na-3s, B-2p, and C-2p orbitals. After adsorption it appears that the valence orbitals of Na-3s broaden and shift towards the unoccupied state indicating ionized Na atoms. On the other hand, the B-2p and C-2p orbitals

appear to shift towards the left which indicates that the electron occupation in the valence band increases. So it can be concluded that when intercalating Na in the heterostructure, the electrons released by Na will be distributed in both layers of borophene and graphene. A similar mechanism occurs in the adsorption of Li on B/G heterostructure [16].

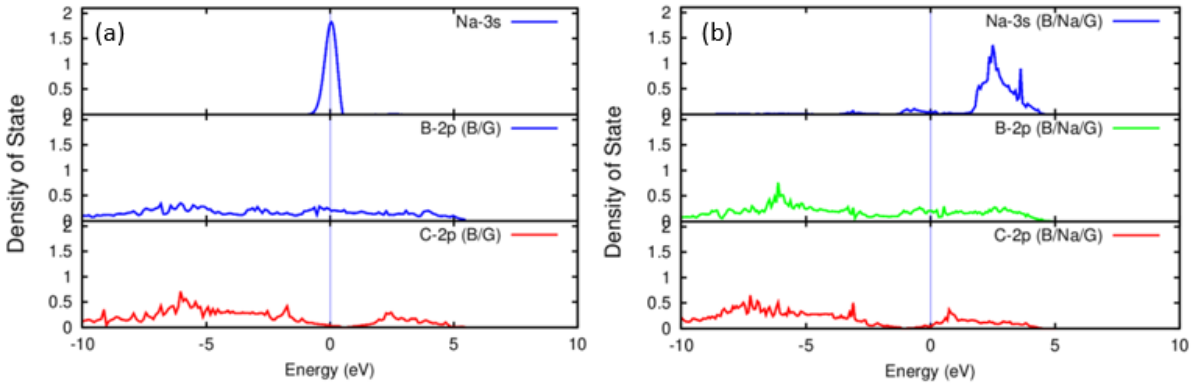

Figure 3. Projected DOS of selected atomic orbital of Na adsorpsi process on heterostructure, (a) before adsorption, and (b) after adsorption.

3.3 Open circuit voltage (VOC) and Theoretical Specific Capacity (TSC)

In the charging process, Na ions are pumped from the cathode to the anode through the electrolyte. The Na ions are then bound to the anode material. The amount of Na (n) ions that can be accommodated in the anode is limited by the ability of the anode to adsorb it. The more Na ions that are adsorbed, the more the adsorption potential energy decreases. The capacity of the anode to store energy is proportional to the maximum number of Na ions that can be adsorbed. In this study, we varied the number of Na ions adsorbed on the heterostructure gradually to obtain the maximum number of adsorbed Na ions. This process is shown in Figure 4. We found that the maximum number of Na ions that are adsorbed strongly enough is 7 Na ions. The adsorption energies for different numbers of adsorbed Na from n=1 to n=7 are -2.02 eV, -1.95 eV, -1.67 eV, -1.37 eV, -1.27 eV, -1.27 eV, and -0.73 eV, respectively.

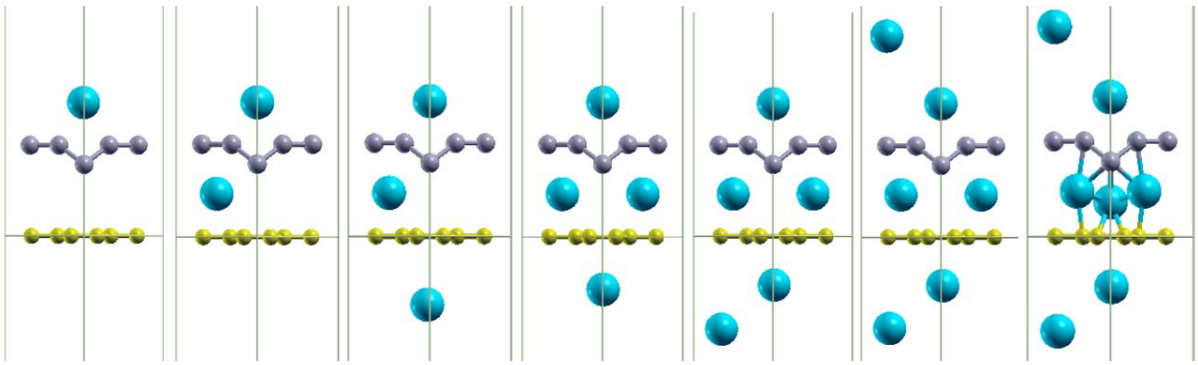

Figure 4. Na Ions Adsorption on B/G heterostructure anode.

The Na storage capacity of the B/G heterostructure anode is calculated based on the maximum number of Na ions adsorbed via equation (5).

$$C = \frac{nvF}{M} \tag{5}$$

where F is the Faraday constant (26801 mAh/mol), M is the molar weight of the B/G unit cell, n is the number of cations adsorbed on the B/G unit, and v is the valence state of the completely ionized cation of the electrolyte. In this case, n is 7 at full coverage, n is 1 for Ni ions and MB/G is 193.48 g/mol. So the Na storage capacity (CB/G) is 969.65 mAh/g. This capacity is greater than the anode based on graphite [7], silicene/BN [10], and G/BP [13] whose values are 150, 306, and 541 $mAhg^{-1}$.

Based on the adsorption potential energy above, the open circuit voltage (OCV) of the B/G heterostructure anode during the charging process is simulated by gradually increasing the adsorption amount of Na ions. OCV B/G heterostructure anode is shown in Figure 5. The OCV of the B/G heterostructure anode is in the range 0.73 – 2.02 V.

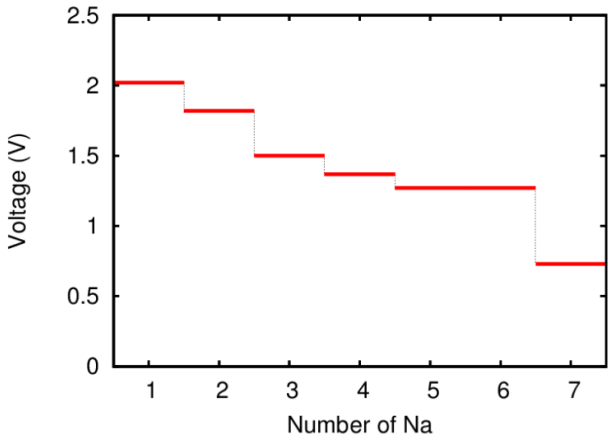

Figure 5. Open circuit voltage (OCV) of B/G heterostructure anode.

3.4 Na Ion Mobility

Na ion mobility refers to how easily Na ions move and diffuse in the battery, in this case, especially in the anode material. The mobility of Na ions is determined by the diffusion barrier which is a potential barrier that inhibits the movement of Na ions. The diffusion barrier is defined as the energy that must be overcome by the ion in order to reach its final position. In this study, we calculated the diffusion barrier for the mobility of Na ions in the B/G interlayer region with the diffusion path chosen as shown in Figure 6a. There are two diffusion paths, namely pathway I and pathway II, where pathway I is the direct path while pathway II there is an intermediate position. The energy diagrams along pathways I and II are shown in Figures 6b and 6c, respectively. Based on equation 4, the diffusion barrier for the two paths is 0.19 eV and 0.16 eV, respectively.

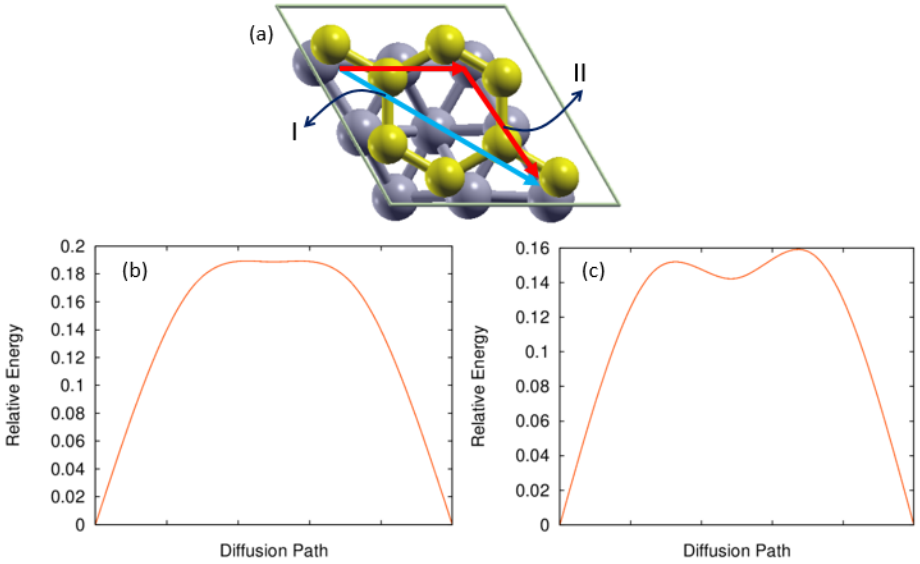

Figure 6. Na Ion mobility in B/G interlayer, (a) diffusion path, (b) energy diagram along path I, (c) energy diagram along path II.

The smaller the diffusion barrier, the greater the rate of diffusion. The diffusion rate can be roughly calculated based on the Arrhenius equation as given in equation 6. The diffusion rate determines the charge-discharge rate and the power density of the ion battery.

$$D = Ae^{(\frac{-E_{barrier}}{kT})} \quad (6)$$

Table 3 compares several heterostructure-based anode properties that were previously reported and the B/G heterostructure of this study. It appears that the B/G heterostructure has superior performance in terms of Na capacity compared to other heterostructures. Apart from the specific properties of the B/G-Na interaction, this advantage can also be directly related to the fairly large interlayer spacing in the B/G heterostructure. Meanwhile, the diffusion barrier of B/G is relatively higher compared to other heterostructures except SnS2/graphene, but this value is much lower than when using a standard graphite anode (~0.59 eV)[22].

Table 3 Direct comparison of anode heterostructure properties of this study and previous work

Anode Materials	Interlayer distance (Å)	VOC (V)	TSC ($mAhg^{-1}$)	Diffusion Barrier (eV)
Silicene/BN [10]	3.36	2.07	306.00	0.0024
BN/Blue-P [17]	3.30	2.03	541.00	0.0700
BN/Black-P [18]	3.34	2.55	445.00	0.0700
G/P [19]	3.50	2.42	580.00	0.0500
VS_2/Ti_2CO_2 [20]	2.81	0.18	601.44	0.0002
VS_2/V_2CO_2 [20]	2.75	0.21	585.29	0.0330
SnS_2/graphene [21]	3.40	1.81	586.00	0.6000
B/G (this work)	3.80, 4.90	2.02	969.65	0.1600

4. CONCLUSIONS

Based on this study, it can be concluded that the Borophene/Graphene (B/G) heterostructure is suitable for use as an anode for Sodium ion batteries. The B/G structure has the farthest interlayer distance of 4.9 Å and the closest at 3.8 Å making it suitable for the passage of Na ions which have an atomic radius of 1.86 Å. With a fairly large Na adsorption energy value of 2.02 eV, the B/G heterostructure can accommodate Na ions up to a specific capacity of 969.65 mAh/g. The diffusion rate of Na ions in the B/G heterostructure interlayer is quite high with a low diffusion barrier below 0.2 eV.

ACKNOWLEDGEMENTS

We acknowledge the support of the Department of Physics, IPB University IPB for high-performance computing (HPC) resources. We also acknowledge funding from the IPB University with project registration number 11419/IT3/PT.01.03/P/B/2023.

REFERENCES

[1] Pan, H., Hu, Y. S., & Chen, L, 2013. Energy and Environmental Science. 6, Issue 8, 2338–2360. https://doi.org/10.1039/c3ee40847g.
[2] Haynes W. M. Handbook of Chemistry and Physics. Florida (US): CRC Press 2016. https://doi.org/10.1201/9781315380476.
[3] Pandit B, Rondiya SR, Dzade NY, Shaikh SF, Kumar N, Goda ES, Al-kahtani AA, Mane RS, Mathur S, Salunkhe RR, 2021. ACS Appl Mater Interfaces. 13 Issue 9, 11433-11441. https://doi.org/10.1021/acsami.0c21081.
[4] Hwang J. Y., Myung S. T., Sun Y. K, 2017. Chem Soc Rev. 46, Issue 12, 3529-3614. https://doi.org/10.1039/c6cs00776g.
[5] Tinambunan, A., Ahmad, F., Sakti, A. W., Putro, P. A., Syafri, & Alatas, H, 2022. Journal of Physical Chemistry C. 126, Issue 49, 20754–20761. https://doi.org/10.1021/acs.jpcc.2c06321.
[6] Lyu, Y., Liu, Y., Yu, Z. E., Su, N., Liu, Y., Li, W., Li, Q., Guo, B., & Liu, B, 2019. Sustainable Materials and Technologies. 21, e00098. https://doi.org/10.1016/j.susmat.2019.e00098.
[7] Luo, W., Shen, F., Bommier, C., Zhu, H., Ji, X., & Hu, L, 2016. Accounts of Chemical Research. 49 Issue 2, 231–240. https://doi.org/10.1021/acs.accounts.5b00482.
[8] Du, Y. T., Kan, X., Yang, F., Gan, L. Y., & Schwingenschlögl, U, 2018. ACS Applied Materials and Interfaces. 10 Issue 38, 32867–32873. https://doi.org/10.1021/acsami.8b10729.
[9] Yankowitz, M., Ma, Q., Jarillo-Herrero, P., & LeRoy, B. J., 2019. Nature Reviews Physics. 1, Issue 2, 112–125. https://doi.org/10.1038/s42254-018-0016-0.
[10] Wang, T., Li, C., Xia, C., Yin, L., An, Y., Wei, S., & Dai, X, 2020. Physica E: Low-Dimensional Systems and Nanostructures. 122, 114146. https://doi.org/10.1016/j.physe.2020.114146.
[11] Liu, X., & Hersam, M, 2019. C. Sci. Adv. 5 Issue 10, eaax6444. https://doi.org/10.1126/sciadv.aax6444.
[12] Lin, Y., Yu, M., Li, X., Gao, W., Wang, L., Zhao, X., Zhou, M., Yao, X., He, M., & Zhang, X, 2021. J. Mater. Chem. C. 9 Issue 44, 15877–15885. https://doi.org/10.1039/D1TC04197E.
[13] Fan, K., Tang, T., Wu, S., & Zhang, Z, 2018. International Journal of Modern Physics B. 32, Issue 1, 1850010. https://doi.org/10.1142/S0217979218500108.
[14] Yang, Z., Li, W., & Zhang, J, 2021. Nanotechnology. 33 Issue 7, 75403. https://doi.org/10.1088/1361-6528/ac3686.
[15] Xiong, Z., Zhong, L., Wang, H., & Li, X, 2021. Materials. 14 Issue 5, 1–43. https://doi.org/10.3390/ma14051192.

[16] Yu, J., Zhou, M., Yang, M., Yang, Q., Zhang, Z., & Zhang, Y, 2020. ACS Applied Energy Materials. 3, Issue 12, 11699–11705. https://doi.org/10.1021/acsaem.0c01808 .

[17] Bao, J., Zhu, L., Wang, H., Han, S., Jin, Y., Zhao, G., Zhu, Y., Guo, X., Hou, J., Yin, H., & Tian, J, 2018. Journal of Physical Chemistry C. 122 Issue 41, 23329–23335. https://doi.org/10.1021/acs.jpcc.8b07062.

[18] Chowdhury, C., Karmakar, S., & Datta, A, 2016. ACS Energy Letters. 1 Issue 1, 253–259. https://doi.org/10.1021/acsenergylett.6b00164.

[19] Mansouri, Z., Sibari, A., Al-Shami, A., Lahbabi, S., el Kenz, A., Benyoussef, A., el Fatimy, A., & Mounkachi, O, 2022. Computational Materials Science. 202, 110936. https://doi.org/10.1016/j.commatsci.2021.110936.

[20] Tang, C., Min, Y., Chen, C., Xu, W., & Xu, L, 2019. Nano Letters. 19, Issue 8, 5577–5586. https://doi.org/10.1021/acs.nanolett.9b02115.

[21] Samad, A., Noor-A-Alam, M., & Shin, Y. H, 2016. Journal of Materials Chemistry A. 4, Issue 37, 14316–14323. https://doi.org/10.1039/c6ta05739j.

[22] Yang, C., Sun, X., Zhang, X., Li, J., Ma, J., Li, Y., Xu, L., Liu, S., Yang, J., Fang, S., Li, Q., Yang, X., Pan, F., Lu, J., & Yu, D, 2021. Carbon. 176, 242–252. https://doi.org/10.1016/j.carbon.2020.12.039.